Available online at www.sciencedirect.com
ScienceDirect
J. Differential Equations 245 (2008) 442–467
Journal of Differential Equations
www.elsevier.com/locate/jde

Bifurcation analysis of a plant–herbivore model with toxin-determined functional response ☆

Rongsong Liu [a], Zhilan Feng [a,*], Huaiping Zhu [b], Donald L. DeAngelis [c]

[a] *Department of Mathematics, Purdue University, West Lafayette, IN 47907, USA*
[b] *Department of Mathematics and Statistics, York University, Toronto, ON M3J 1P3, Canada*
[c] *Department of Biology, University of Miami, Coral Gables, FL 33124, USA*

Received 12 July 2007

Available online 3 December 2007

Abstract

A system of ordinary differential equations is considered which models the plant–herbivore interactions mediated by a toxin-determined functional response. The new functional response is a modification of the traditional Holling Type II functional response by explicitly including a reduction in the consumption of plants by the herbivore due to chemical defenses. A detailed bifurcation analysis of the system reveals a rich array of possible behaviors including cyclical dynamics through Hopf bifurcations and homoclinic bifurcation. The results are obtained not only analytically but also confirmed and extended numerically.

Keywords: Plant–herbivore model; Stability; Limit cycle; Homoclinic bifurcation

1. Introduction

Plant–herbivore interactions have been studied previously by many researchers using differential equations and theories in dynamical systems. One of the most commonly employed descriptions of the plant consumption by the herbivore is the traditional Holling Type II functional response [5,6], which assumes that the growth rate of herbivore is a monotonically increasing

☆ This work is supported in part by James S. McDonnell Foundation 21st Century Science Initiative and NSF grant DMS-0719697 (ZF). DLD's contribution was supported by the US Geological Survey's Greater Everglades Priority Ecosystem Science program and USGS's Florida Integrated Science Center.

* Corresponding author.
E-mail addresses: rliu@math.purdue.edu (R. Liu), zfeng@math.purdue.edu (Z. Feng), huaiping@mathstat.yorku.ca (H. Zhu), ddeangelis@bio.miami.edu (D.L. DeAngelis).

0022-0396/$ – see front matter
doi:10.1016/j.jde.2007.10.034

function of plant density. However, this will not be appropriate if the chemical defense of plants is considered, in which case the negative effect of plant toxin on herbivore can lead to a decrease in the growth rate when the plant density is high.

To explore the impact of plant toxicity on the dynamics of plant–herbivore interactions, we developed ordinary differential equation models that include a toxin-determined functional response (see [4,8]). The toxin-determined functional response is a modification of the traditional Holling Type II response by including the negative effect of toxin on herbivore growth, which can overwhelm the positive effect of biomass ingestion at sufficiently high plant toxicant concentrations [2,3].

The inclusion of plant toxicity in the functional response makes the equations highly nonlinear with much more complex dynamics. The model considered in [8] is a 3-dimensional system which includes one herbivore population and two plant species with different levels of toxicity and competition ability. Numerical studies of that model show that the system exhibits Hopf and period doubling bifurcations for parameter values in certain regions. Analysis of the 3-D system seems to be very difficult and hence mathematical results obtained in [8] are very limited.

In [4], a simpler 2-D model is considered which includes only one plant species and one herbivore population. The 2-dimensional system reads:

$$\begin{aligned} \frac{dN}{dt} &= rN\left(1-\frac{N}{K}\right) - C(N)P, \\ \frac{dP}{dt} &= BC(N)P - dP, \end{aligned} \tag{1.1}$$

where

$$C(N) = f(N)\left(1-\frac{f(N)}{4G}\right) \tag{1.2}$$

and $f(N)$ is the Holling Type II functional response given by

$$f(N) = \frac{e\sigma N}{1+he\sigma N}. \tag{1.3}$$

e is the encounter rate, which depends on the movement velocity of the consumer and its radius of detection of food items. The parameter σ $(0 < \sigma \leqslant 1)$ is the fraction of food items encountered that the herbivore ingests which may be a function of N, while h is the handling time for each prey item, which incorporates the time required for the digestive tract to handle the item. B is the conversion of consumed plant biomass into new herbivore biomass (through both growth and reproduction), d is the per capita rate of herbivore death due to causes unrelated to plant toxicity, r is the plant intrinsic growth rate, and K is the carrying capacity. All parameters and their units are defined in Table 1.

As the article [4] is intended to be more biologically oriented, it focused on the model description of outcomes and omitted most of the mathematical analyses. In this paper, we provide a detailed bifurcation analysis of the system (1.1).

To see clearly the role of plant toxin and herbivore browsing, we choose G and d to be the bifurcation parameters. Notice that G measures the toxicity level and d reflects intensity of herbivory. We show that there exists a Hopf bifurcation curve, $d = d_{\text{hopf}}(G)$, such that an interior equilibrium loses its stability when d passes the curve and a stable periodic solution appears. We

Table 1
Definition of parameters used in model (1.1)

Parameter	Definition
r	Intrinsic growth rate of plant
T	Amount of toxin contained per unit plant
M	Max amount of toxin a herbivore can consume per unit time
G	$= M/T$
h	Time for handling one unit of plant
e	Rate of encounter per unit plant
σ	Fraction of food items encountered that the herbivore ingests
B	Conversion constant (herbivore biomass per unit of plant)
K	Carrying capacity of plant
α	Scaling constant
d	Per capital death rate of herbivore unrelated to plant toxicity

also show that the system has a codimension two bifurcation at a point $(\hat{G}, \hat{d})$ and determine a homoclinic bifurcation curve, $d = d_{\text{hom}}(G)$, such that the limit cycle disappears when d passes the curve. This bifurcation is not present in models with Holling Type II functional response or other functional response models of plant–mammal interactions (e.g., [1,9,10,13]).

Another interesting behavior of system (1.1) is that bi-stable attractors are possible. For example, the system has two stable equilibria for (G, d) in a certain region, or one stable limit cycle and one stable equilibrium for (G, d) in another region. These dynamics represent important implications of the toxin-determined functional response (see [4]).

As done in [4], we consider two cases in terms of the function $\sigma(N)$. One is the case in which $\sigma(N)$ is a constant, which assumes that, although the herbivore's rate of ingestion of plant biomass is negatively affected by increasing ingestion of toxicant relative to the load it can safely deal with, the herbivore is not able to prevent lethal levels in toxicant intake. The other case is when $\sigma(N)$ is not constant, which incorporates the adaptation of the herbivore to control its rate of consumption of plant items when that is likely to lead to lethal toxicant intake. These two cases generate dramatically different outcomes (see the bifurcation diagrams).

This paper is organized as follows. Analysis of the model for the case when $\sigma(N)$ is a constant is given in Section 2. Section 3 considers the case when $\sigma(N)$ is not constant, and Section 4 discusses the results and future work.

2. Analysis of model (1.1) when σ is constant

As discussed in [8], in order for the consumption function $C(N)$ to be nonnegative and below the maximum consumption rate $1/h$, we have the following constraint on G:

$$\frac{1}{4h} < G < \frac{1}{h}. \tag{2.1}$$

For constant $\sigma(N) = \sigma_0$, $C(N)$ is either monotonically increasing, reaching an asymptote (see Fig. 1(a)) for $\frac{1}{4h} < G < \frac{1}{2h}$, or unimodal, declining to an asymptote after reaching a peak G at N_m, where

$$N_m = \frac{2G}{e\sigma_0(1 - 2hG)}, \tag{2.2}$$

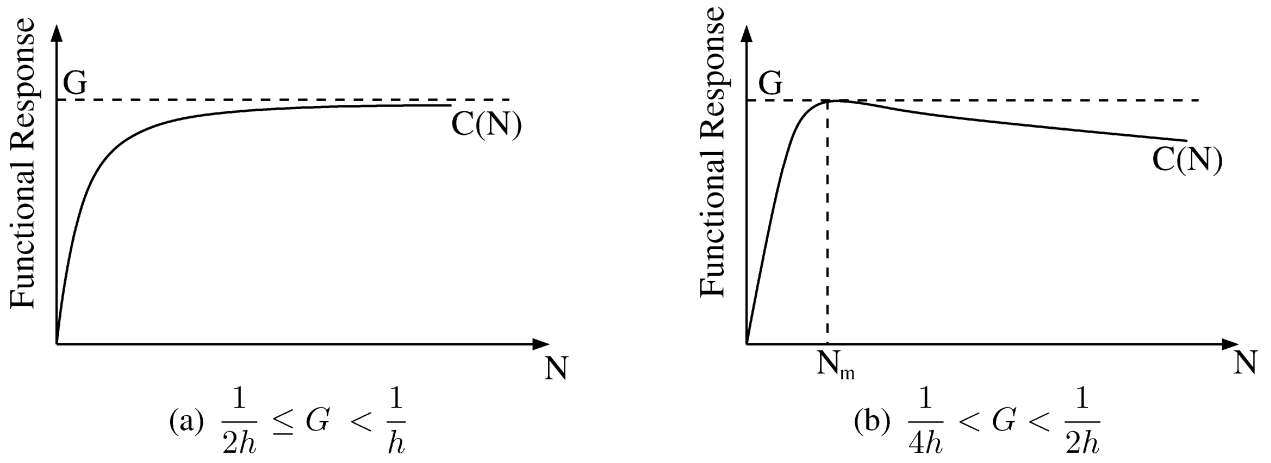

Fig. 1. Graphs of the functional response $C(N)$. (a) $C(N)$ is monotonically increasing. (b) $C(N)$ is unimodal and reaches maximum at $N_m = \frac{2G}{e\sigma_0(1-2hG)}$.

for $\frac{1}{2h} < G < \frac{1}{h}$ (see Fig. 1(b)). The case when $C(N)$ is monotone, i.e., when $\frac{1}{4h} < G < \frac{1}{2h}$, has been analyzed in [8]. In this paper, we are concerned with only the case when $C(N)$ is unimodal, i.e., when $\frac{1}{2h} < G < \frac{1}{h}$.

2.1. Equilibria

System (1.1) always has two boundary equilibria:

$$E_0 = (N, P) = (0, 0) \quad \text{and} \quad E_K = (K, 0).$$

Besides E_0 and E_K, there may be up to two interior equilibria. Denote an interior equilibrium by $E^* = (N^*, P^*)$ with $N^* > 0$ and $P^* > 0$. For ease of presentation, introduce the function $g(N)$:

$$g(N) = \frac{rN(1 - N/K)}{C(N)}. \tag{2.3}$$

Then, E^* can be determined by solving for N and P using the equations

$$BC(N) - d = 0, \qquad g(N) - P = 0. \tag{2.4}$$

Clearly, for E^* to be biologically feasible, we require

$$0 < N^* < K, \qquad P^* > 0.$$

Rewrite $g(N)$ as

$$g(N) = \frac{r(K - N)(1 + he\sigma_0 N)^2}{e\sigma_0 K(1 + bN)} \quad \text{with } b = e\sigma_0\left(h - \frac{1}{4G}\right), \tag{2.5}$$

and notice the following properties of $g(N)$ for later use: (i) $g(N)$ intersects the positive N-axis at a single point $N = K$ and the intersection with the P-axis is positive; (ii) it has a single hump (maximum) at a point $N_h \in (0, K)$; and (iii) $g(K) = 0$ and $g'(K) < 0$. A graph of $g(N)$ is sketched in Fig. 2.

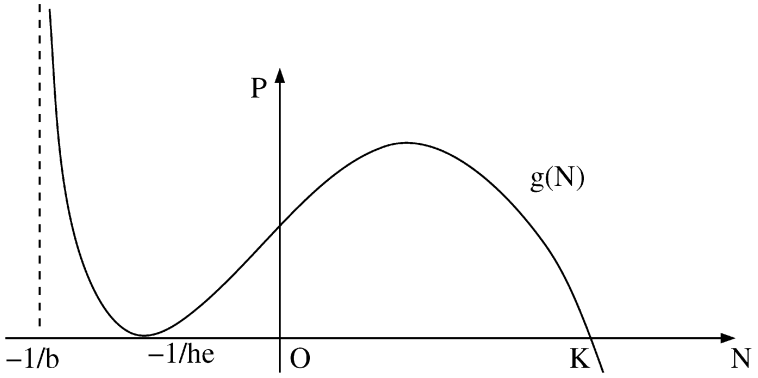

Fig. 2. Plot of the function $g(N)$. It has a single hump for $N \in (0, K)$ with $g(K) = 0$ and $g'(K) < 0$.

The existence of E^* depends on several parameters. To investigate the impact of plant toxicity and herbivore browsing, we choose G and d as our bifurcation parameters and consider bifurcations in the (G, d) plane. To solve (2.4) for N, we use the equation $BC(N) - d = 0$, which is equivalent to the following quadratic equation

$$c_2 N^2 + c_1 N + c_0 = 0, \tag{2.6}$$

where

$$c_0 = -dG, \qquad c_1 = e\sigma_0 G(B - 2dh), \qquad c_2 = (e\sigma_0)^2\big(BhG - B/4 - dh^2 G\big).$$

The discriminant of (2.6) is $\Delta_v = BG(BG - d)$. Thus, (2.6) has real solutions if and only if $d < BG$, which provides a threshold line:

$$\bar{d}(G) = BG. \tag{2.7}$$

(2.6) has two (one or zero) real solutions (provided that $c_2 \neq 0$) when $d < \bar{d}$ ($= \bar{d}$ or $> \bar{d}$), which we denote by N_1 and N_2 with $N_1 < N_2$. In the following, we will only consider the region

$$\Omega = \left\{(G, d) \;\middle|\; \frac{1}{4h} < G < \frac{1}{2h},\ 0 \leqslant d \leqslant \bar{d}(G)\right\}. \tag{2.8}$$

For $(G, d) \in \Omega$, Eq. (2.6) has two solutions:

$$N_1^* = \frac{G(B - 2dh) - \sqrt{\Delta_v}}{2e\sigma_0(\frac{B}{4} + dh^2 G - BhG)}, \qquad N_2^* = \frac{G(B - 2dh) + \sqrt{\Delta_v}}{2e\sigma_0(\frac{B}{4} + dh^2 G - BhG)}. \tag{2.9}$$

Recall that the interior equilibrium $E_i^* = (N_i^*, P_i^*)$, where $P_i^* = g(N_i^*)$, exists if and only if $N_i^* \in (0, K)$ for $i = 1$ or 2. Using this constraint we can get another threshold condition. Let N_m denote the plant population size at which $C(N)$ has its maximum value, G, then

$$N_m = \frac{2G}{e\sigma_0(1 - 2hG)}$$

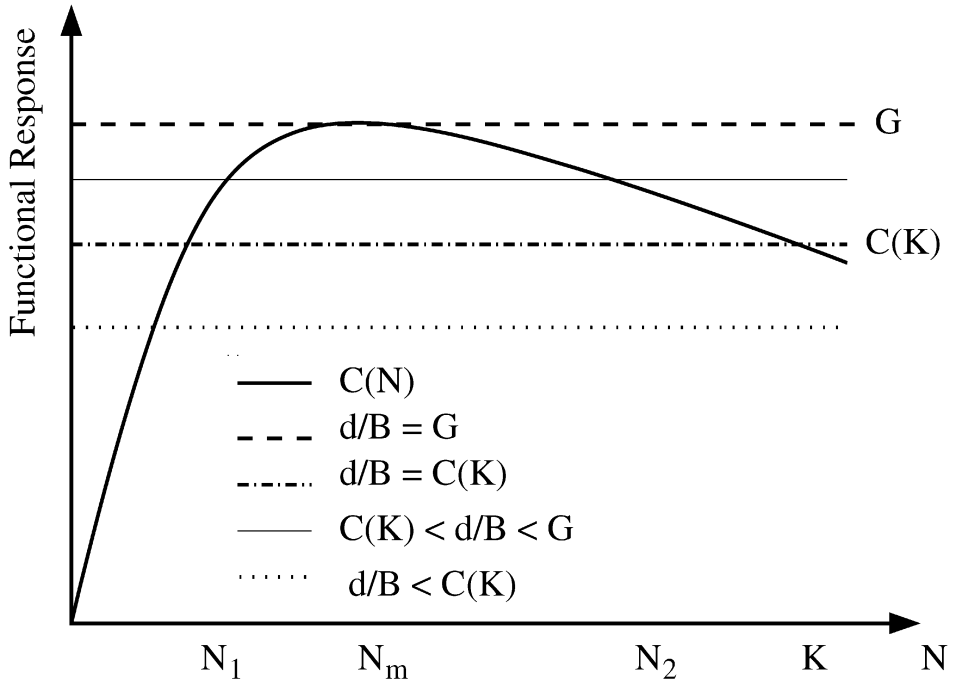

Fig. 3. The N^* component of an interior equilibrium is shown as an intersection of the curve $C(N)$ with a horizontal line d/B. If d/B is between the values of $C(K)$ and G then there are two intersections N_1^* and N_2^* in $(0, K)$, corresponding to two interior equilibria. If d/B is smaller than $C(K)$ then there is only one intersection N_1^* in $(0, K)$ (not labeled), corresponding to the unique interior equilibrium.

(see Fig. 3). From Fig. 3 we see that the number of solutions of (2.6) in $(0, K)$ also depends on the relation between N_m and K. Therefore, the condition $N_m = K$ determines a threshold value $G = G_c$:

$$G_c = \frac{e\sigma_0 K}{2(1 + he\sigma_0 K)}, \tag{2.10}$$

such that

$$N_m < (= \text{or } >)\, K \quad \text{if and only if} \quad G < (= \text{ or } >)\, G_c.$$

Clearly, $G_c < 1/2h$. It is easy to verify that

$$G_c > \frac{1}{4h} \quad \text{if and only if} \quad K > \frac{1}{he\sigma_0}. \tag{2.11}$$

Condition (2.11) is easy to satisfy if the carrying capacity K is large.

If $G < G_c$, then $N_m < K$. In this case, we always have $N_1 \in (0, K)$, and hence, E_1^* always exists. E_2^* exists if only if $N_2 < K$. Thus, by setting $N_2 = K$, which is equivalent to $BC(K) = d$, we get the threshold curve $d = d_K(G)$ with

$$d_K(G) = \frac{BeK(G(1 + e\sigma_0 Kh) - e\sigma_0 K/4)}{G(1 + e\sigma_0 Kh)^2}, \tag{2.12}$$

such that $N_2 < K$ if and only if $d > d_K$. Thus, both E_1^* and E_2^* exist for $d > d_K$ and only E_1^* exists for $d \leqslant d_K$.

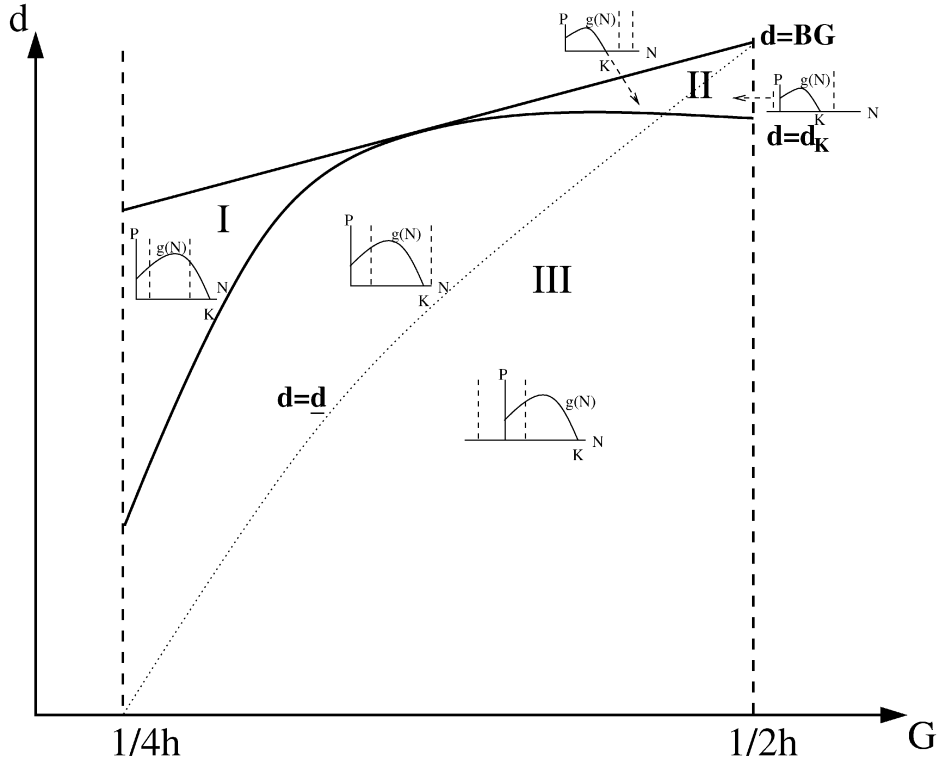

Fig. 4. Existence of interior equilibria. An interior equilibrium $E^* = (N^*, P^*)$ is an intersection of the $g(N)$ curve with a dashed vertical line (see the inserted graphs on the (N, P) plane). It shows that there are two positive equilibria in region I and none in II. In region III, there is only one interior equilibrium as the second intersection has the N-coordinate either < 0 or $> K$.

If $G > G_c$, then $N_m > K$. In this case, E_2^* does not exist, and E_1^* exists if and only if $d < d_K(G)$.

We can show that the curve $d_K(G)$ has the following properties: (i) it is monotonically increasing; (ii) $0 < d_K(G) < \bar{d}(G)$ for $G \in (1/4h, 1/2h)$; and (iii) it intersects $\bar{d}(G)$ at G_c. We remark that the condition $c_2 = 0$ yields another curve,

$$d = \underline{d}(G) = \frac{B(hG - 1/4)}{h^2 G},$$

such that the nature of solutions of (2.6) may be different when (G, d) crosses the curve. However, it does not affect the number of interior equilibrium points (or their stability). From these properties, we can sketch the curve $d_K(G)$ as shown in Fig. 4. This figure also illustrates that the threshold curves, $\bar{d}(G)$ and $d_K(G)$, divide the region Ω into three sub-regions: I, II and III. The number of interior equilibrium points in each of these regions are also shown in Fig. 4 and summarized in Table 2.

2.2. Local stability of equilibria and Hopf bifurcation

We now examine the stability of the equilibria identified above. The variational matrix about any equilibrium $\bar{E} = (\bar{N}, \bar{P})$ of system (1.1) is

$$J(\bar{E}) = \begin{pmatrix} C'(\bar{N})(g(\bar{N}) - \bar{P}) + C(\bar{N})g'(\bar{N}) & -C(\bar{N}) \\ BC'(\bar{N})\bar{P} & BC(\bar{N}) - d \end{pmatrix}. \tag{2.13}$$

Table 2
Linear analysis of equilibrium points

Equilibrium	*I*	*II*	*III*
E_0	saddle	saddle	saddle
E_1^*	repeller if $g'(N_1^*) > 0$	does not exist	repeller if $g'(N_1^*) > 0$
	attractor if $g'(N_1^*) < 0$		attractor if $g'(N_1^*) < 0$
E_2^*	does not exist	does not exist	saddle
E_K	saddle	attracting node	attracting node

It is easy to show that E_0 is always a saddle point. The Jacobian at $E_K = (K, 0)$ is

$$J(E_K) = \begin{pmatrix} C(K)g'(K) & -C(K) \\ 0 & BC(K) - d \end{pmatrix}. \tag{2.14}$$

From $C(K)g'(K) < 0$ (see Fig. 2) we know that a transcritical bifurcation occurs along the curve $d_K(G) = BC(K)$. E_K is an attracting node if $d > d_K$, and it is a saddle if $d < d_K$.

The Jacobian at E_1^* is

$$J\big(E_1^*\big) = \begin{pmatrix} C(N_1^*)g'(N_1^*) & -C(N_1^*) \\ BC'(N_1^*)P_1^* & 0 \end{pmatrix}. \tag{2.15}$$

Clearly, $\det J(E_1^*) > 0$ as $C(N_1^*) > 0$ and $C'(N_1^*) > 0$. Notice that

$$\operatorname{tr} J\big(E_1^*\big) = C\big(N_1^*\big)g'\big(N_1^*\big).$$

Hence, E_1^* is an attractor if $g'(N_1^*) < 0$ and it is a repeller if $g'(N_1^*) > 0$.

The stability switch of E_1^* suggests the possibility of a Hopf bifurcation. Since N_1^* is a function of G and d, we can determine a Hopf curve $d = d_{\text{hopf}}(G)$ by solving the equations

$$BC\big(N_1^*\big) - d = 0, \qquad g'\big(N_1^*\big) = 0. \tag{2.16}$$

Note that

$$g'(N) = -\frac{r}{e\sigma_0 K}\frac{(1 + he\sigma_0 N)G(a_2N^2 + a_1N + a_0)}{(G + e\sigma_0 N(hG - 1/4))^2}, \tag{2.17}$$

where

$$\begin{aligned} a_0 &= G - he\sigma_0 KG - e\sigma_0 K/4, \\ a_1 &= -e\sigma_0 h(he\sigma_0 KG - e\sigma_0 K/4 - 3G), \\ a_2 &= 2(e\sigma_0)^2 h(hG - 1/4). \end{aligned} \tag{2.18}$$

It can be verified that the discriminant of $g'(N) = 0$,

$$\Delta_g = h(G + he\sigma_0 KG - e\sigma_0 K/4)\big(2 + hG + e\sigma_0 h^2 KG - e\sigma_0 hK/4\big), \tag{2.19}$$

is positive. Notice that N_1^* is the larger critical point of $g(N)$ (the smaller one is negative), which is given by

$$N_1^* = \frac{-a_1 + \sqrt{\Delta_g}}{2a_2}. \tag{2.20}$$

From Eq. (2.6) we also have

$$N_1^* = \frac{G(B - 2dh) - \sqrt{\Delta_v}}{2e\sigma_0(B/4 + dh^2G - BhG)}, \tag{2.21}$$

where $\Delta_v = BG(BG - d) > 0$. Setting the two expressions in (2.20) and (2.21) equal we obtain the curve

$$\begin{aligned} d &= d_{\text{hopf}}(G) \\ &= \frac{B}{2hG(1 + e\sigma_0 hK)^2}\left[\left(G + e\sigma_0 hGK - \frac{e\sigma_0 K}{4}\right)\right. \\ &\quad \left.\times\left(\frac{5e\sigma_0 hK}{4} - 1 + hG + h^2 e\sigma_0 GK\right) - \left(e\sigma_0 hGK + G - \frac{3e\sigma_0 K}{4}\right)\sqrt{\Delta_g}\right]. \end{aligned} \tag{2.22}$$

It is easy to check that the curves $d_{\text{hopf}}(G)$ and $\bar{d}(G)$ intersect at $G = \hat{G}$, where

$$\hat{G} = \frac{e\sigma_0 K}{2(2 + he\sigma_0 K)} < \frac{e\sigma_0 K}{2(1 + he\sigma_0 K)} = G_c. \tag{2.23}$$

In order to have $\hat{G} > \frac{1}{4h}$ we also need to require $K > \frac{2}{e\sigma_0 h}$. The graph of $d_{\text{hopf}}(G)$ is shown in Fig. 5.

To confirm that a Hopf bifurcation indeed occurs along the curve $d_{\text{hopf}}(G)$, it suffices to check the sign of the Liapunov coefficient, θ, which for the system (1.1) is given by

$$\theta(N) = -\frac{C(N)g''(N)C''(N)}{C'(N)} + C(N)g'''(N) + 2C'(N)g''(N) \tag{2.24}$$

(see [14,15]). Using (2.20) and (2.21) (with N replaced by N_1^*) we can rewrite (2.24) as

$$\theta\big(N_1^*\big) = \frac{g''(N_1^*)}{C'(N_1^*)}\big(2C'^2\big(N_1^*\big) - C\big(N_1^*\big)C''\big(N_1^*\big)\big) + C\big(N_1^*\big)g'''\big(N_1^*\big).$$

After checking that $C(N_1^*) > 0$, $C'(N_1^*) > 0$, $C''(N_1^*) < 0$, $g''(N_1^*) < 0$ and $g'''(N_1^*) < 0$, we have that $\theta(N_1^*) < 0$. It follows that a Hopf bifurcation occurs along the curve $d_{\text{hopf}}(G)$ and it is supercritical. Thus, we have proved the following theorem.

Theorem 1. *A supercritical Hopf bifurcation occurs along the curve $d = d_{\text{hopf}}(G)$ for $\hat{G} < G < 1/2h$.*

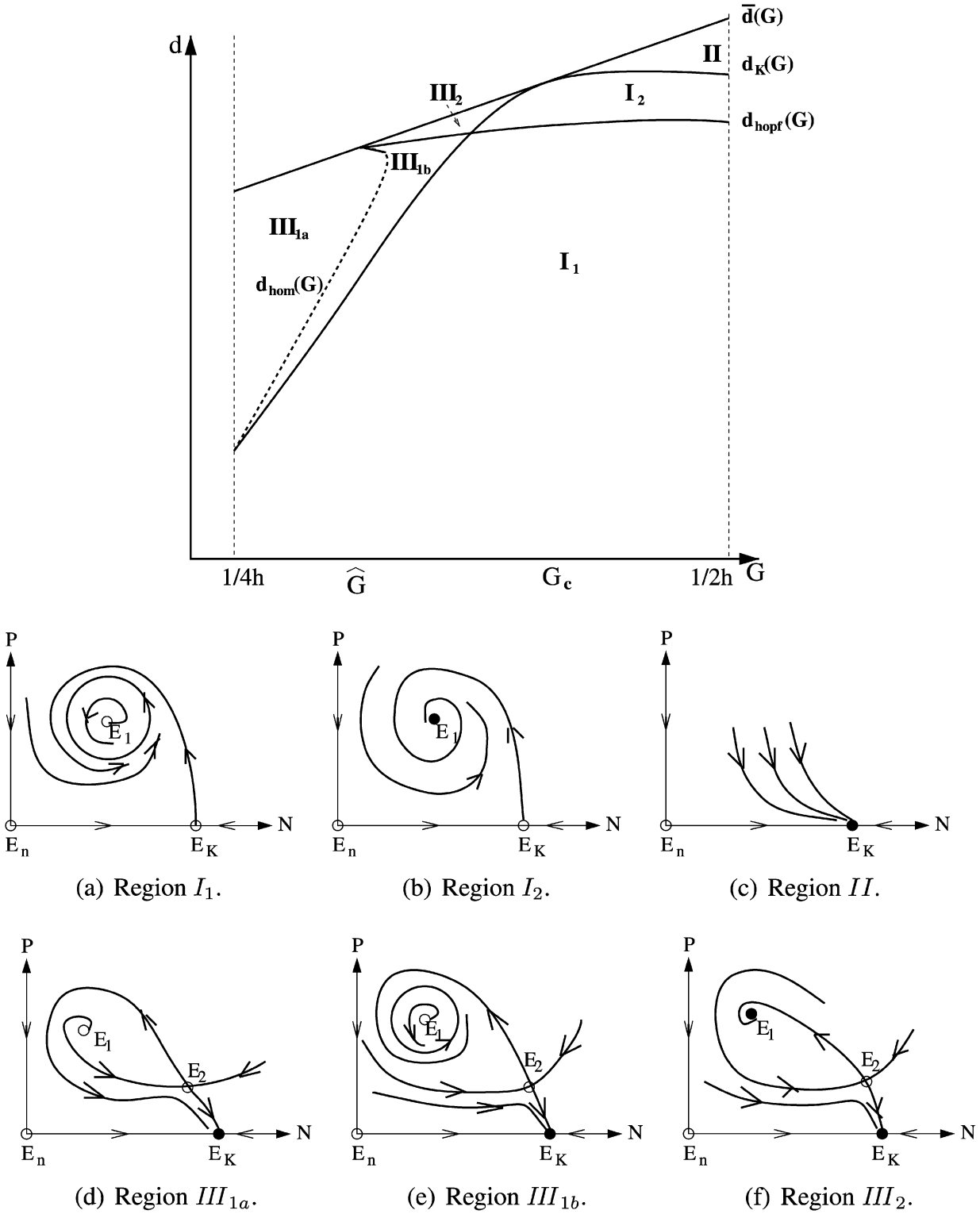

(a) Region I_1. (b) Region I_2. (c) Region II.

(d) Region III_{1a}. (e) Region III_{1b}. (f) Region III_2.

Fig. 5. The top panel is a bifurcation diagram for the case where $\sigma(N)$ is constant. (a)–(f) are phase portraits in each region. A circle represents an unstable equilibrium and a solid dot represents a stable equilibrium.

For the stability of E_2^*, noticing that $N_2^* > N_m$ and hence $C'(N_2^*) < 0$, we know that

$$\det J\left(E_2^*\right) = BC'\left(N_2^*\right)C\left(N_2^*\right)P_2^* < 0.$$

Therefore, E_2^* is a saddle point whenever it exists.

The stability results obtained above are summarized in Table 2 and illustrated in Fig. 5, which is a bifurcation diagram. Figure 5 includes also additional bifurcations that will be discussed in the next section.

2.3. The cusp point of codimension 2

Notice that the saddle node bifurcation curve, $d = \bar{d}(G)$, and the Hopf bifurcation curve, $d = d_{\text{hopf}}(G)$, intersects at $G = \hat{G}$. This suggests that the point

$$O_p = (\hat{G}, \hat{d}), \quad \text{with } \hat{d} = \bar{d}(\hat{G}) = d_{\text{hopf}}(\hat{G}), \tag{2.25}$$

is an organizing center at which a codimension two bifurcation may occur. Recall that for $1/4h < \hat{G} < 1/2h$ we require that $K > \frac{2}{e\sigma_0 h}$, which will be assumed throughout this section. Since $E_1^* = E_2^*$ at O_p, to simplify the notation we denote $N_1^* = N_2^*$ by N^* and $P^* = g(N^*)$. Then, $g'(N^*) = 0$.

Theorem 2. *For $(G, d) = (\hat{G}, \hat{d})$ the system* (1.1) *has a cusp point of codimension* 2 (*a Takens–Bogdanov bifurcation*) *at $E^* = (N^*, P^*)$.*

To prove Theorem 2, we first prove the following lemma.

Lemma 1. *For all $N > 0$, if $g'(N) = 0$ then $g''(N) \neq 0$.*

Proof. It is easy to check that for all N

$$g''(N) = -\frac{r}{e\sigma_0 K} \frac{2Ge\sigma_0(b_3N^3 + b_2N^2 + b_1N + b_0)}{(G + e\sigma_0 N(hG - 1/4))^3}, \tag{2.26}$$

with

$$\begin{aligned} b_3 &= h^2(e\sigma_0)^3(hG - 1/4)^2, \\ b_2 &= 3h^2(e\sigma_0)^2G(hG - 1/4), \\ b_1 &= 3e\sigma_0h^2G^2, \\ b_0 &= G/4 - e\sigma_0K/16 + hG^2. \end{aligned}$$

Solving $g'(N) = 0$ with $N > 0$ we have that

$$N = \frac{-a_1/e\sigma_0 + \sqrt{\Delta_g}}{2a_2/e\sigma_0} > 0, \tag{2.27}$$

where Δ_g is given by expression (2.19). Substituting the expression (2.27) for N in (2.26) we find that $g''(N) \neq 0$. Therefore, the lemma is proved. □

We now prove Theorem 2.

Proof of Theorem 2. Let $\bar{C}(N)$ and $\bar{g}(N)$ denote, respectively, $C(N)$ and $g(N)$ with G replaced by $\hat{G}$, i.e.,

$$\bar{C}(N) = \frac{e\sigma_0 N}{1+he\sigma_0 N}\left(1 - \frac{e\sigma_0 N}{4\hat{G}(1+he\sigma_0 N)}\right),$$
$$\bar{g}(N) = \frac{r}{e\sigma_0 K}\frac{(K-N)(1+he\sigma_0 N)^2}{1+(h-e\sigma_0/4\hat{G})N}. \tag{2.28}$$

Notice that

$$N^* = \frac{2\hat{G}}{e(1-2h\hat{G})}, \qquad P^* = \bar{g}(N^*), \tag{2.29}$$

and that

$$\bar{C}'(N^*) = 0, \qquad \bar{g}'(N^*) = 0.$$

Thus, the Jacobian (2.13) at $E^* = (N^*, P^*)$ has double zero eigenvalues.

Consider the transformation

$$x_1 = N - N^*, \qquad x_2 = P - P^*. \tag{2.30}$$

Then at O_p system (1.1) becomes

$$\frac{dx_1}{dt} = \bar{C}(N^*)x_2 + \frac{1}{2}\bar{C}(N^*)\bar{g}''(N^*)x_1^2 + R_{10}(x_1, x_2),$$
$$\frac{dx_2}{dt} = \frac{1}{2}B\bar{C}''(N^*)P^*x_1^2 + R_{20}(x_1, x_2), \tag{2.31}$$

where $R_{i0}(x_1, x_2)$ $(i = 1, 2)$ is C^∞ and $R_{i0}(x_1, x_2) = O(|(x_1, x_2)|^3)$. From another transformation,

$$y_1 = x_1, \qquad y_2 = \bar{C}(N^*)x_2, \tag{2.32}$$

system (2.31) becomes

$$\frac{dy_1}{dt} = y_2 + \frac{1}{2}\bar{C}(N^*)\bar{g}''(N^*)y_1^2 + R_{11}(y_1, y_2),$$
$$\frac{dy_2}{dt} = \frac{1}{2}B\bar{C}(N^*)\bar{C}''(N^*)P^*y_1^2 + R_{21}(y_1, y_2),$$

where $R_{i1}(y_1, y_2)$ $(i = 1, 2)$ is C^∞ and $R_{i1}(y_1, y_2) = O(|(y_1, y_2)|^3)$. Finally, using the near-identity transformation,

$$u = y_1, \qquad v = y_2 + \frac{1}{2}\bar{C}(N^*)\bar{g}''(N^*)y_1^2 + R_{11}(y_1, y_2), \tag{2.33}$$

we obtain

$$\frac{du}{dt} = v,$$
$$\frac{dv}{dt} = \delta_1 u^2 + \delta_2 uv + R_{22}(u, v),$$

where $R_{22}(u, v) = O(|(u, v)|^3)$ is C^∞ and

$$\delta_1 = \frac{1}{2} B\bar{C}(N^*)\bar{C}''(N^*)P^* < 0, \qquad \delta_2 = \bar{C}(N^*)\bar{g}''(N^*) < 0,$$

from Lemma 1. By applying Theorem 8.4 in [7], we complete the proof of Theorem 2. □

The next result shows that the original system (1.1) is a generic unfolding of the singularity at $O_p = (\hat{G}, \hat{d})$.

Theorem 3. *For (G, d) sufficiently close to $(\hat{G}, \hat{d})$ the system* (1.1) *is a generic unfolding of the cusp singularity of codimension* 2 *at $(\hat{G}, \hat{d})$.*

Proof. Let

$$G = \hat{G} + \epsilon_1, \qquad d = \hat{d} + \epsilon_2, \tag{2.34}$$

where ϵ_1 and ϵ_2 are small numbers. Then (1.1) can be written as

$$\frac{dN}{dt} = C(N, \epsilon_1)\big(g(N, \epsilon_1) - P\big),$$
$$\frac{dP}{dt} = BC(N, \epsilon_1)P - (d + \epsilon_2)P, \tag{2.35}$$

with

$$C(N, \epsilon_1) = \frac{e\sigma_0 N}{1 + he\sigma_0 N}\left(1 - \frac{e\sigma_0 N}{4(\hat{G} + \epsilon_1)(1 + he\sigma_0 N)}\right),$$
$$g(N, \epsilon_1) = \frac{r}{e\sigma_0 K}\frac{(K - N)(1 + he\sigma_0 N)^2}{1 + \big(h - \frac{e\sigma_0}{4(\hat{G}+\epsilon_1)}\big)N}. \tag{2.36}$$

From Theorem 2 we know that system (2.35) has a cusp point at E^* if $\epsilon = 0$. By using the transformation (2.30), system (2.35) becomes

$$\begin{aligned}\frac{dx_1}{dt} &= C(N^*, 0)x_2 + a_{00}(\epsilon) + a_{10}(\epsilon)x_1 + a_{01}(\epsilon)x_2 + \frac{1}{2}a_{20}(\epsilon)x_1^2 \\ &\quad + a_{11}(\epsilon)x_1x_2 + P_{10}(x_1, x_2, \epsilon), \\ \frac{dx_2}{dt} &= b_{00}(\epsilon) + b_{10}(\epsilon)x_1 + b_{01}(\epsilon)x_2 + \frac{1}{2}b_{20}(\epsilon)x_1^2 + b_{11}(\epsilon)x_1x_2 \\ &\quad + P_{20}(x_1, x_2, \epsilon),\end{aligned} \tag{2.37}$$

where $P_{i0}(x_1, x_2, \epsilon)$ $(i = 1, 2)$ is C^∞ and $P_{i0}(x_1, x_2, \epsilon) = O(|(x_1, x_2)|^3)$, and

$$
\begin{aligned}
a_{00} &= C(N^*, \epsilon_1)\big(g(N^*, \epsilon_1) - P^*\big),\\
a_{10} &= C(N^*, \epsilon_1)g'(N^*, \epsilon_1),\\
a_{01} &= \epsilon_1 \frac{\partial C(N^*, \epsilon_1)}{\partial \epsilon_1}\bigg|_{\epsilon_1=0} + O\big(\epsilon^2\big),\\
a_{20} &= C''(N^*, \epsilon_1)\big(g(N^*, \epsilon_1) - P^*\big) + 2C'(N^*, \epsilon_1)g'(N^*, \epsilon_1) + C(N^*, \epsilon_1)g''(N^*, \epsilon_1),\\
a_{11} &= -C'(N^*, \epsilon_1),\\
b_{00} &= \big(BC(N^*, \epsilon_1) - (d + \epsilon_2)\big)P^*,\\
b_{10} &= BC'(N^*, \epsilon_1)P^*,\\
b_{01} &= BC(N^*, \epsilon_1) - (d + \epsilon_2),\\
b_{20} &= BC''(N^*, \epsilon_1)P^*,\\
b_{11} &= BC'(N^*, \epsilon_1).
\end{aligned}
$$

Here '′' and '″' denote the derivatives of the functions g and C with respect to N.

From the transformation (2.32), the above system becomes

$$
\begin{aligned}
\frac{dy_1}{dt} &= y_2 + a_{00}(\epsilon) + a_{10}(\epsilon)y_1 + \frac{a_{01}(\epsilon)}{C(N^*, 0)}y_2 + \frac{1}{2}a_{20}(\epsilon)y_1^2 + \frac{a_{11}(\epsilon)}{C(N^*, 0)}y_1y_2\\
&\quad + P_{11}(y_1, y_2, \epsilon),\\
\frac{dy_2}{dt} &= b_{00}(\epsilon)C(N^*, 0) + b_{10}(\epsilon)C(N^*, 0)y_1 + b_{01}(\epsilon)y_2 + \frac{1}{2}b_{20}(\epsilon)C(N^*, 0)y_1^2\\
&\quad + b_{11}(\epsilon)y_1y_2 + P_{21}(y_1, y_2, \epsilon),
\end{aligned}
\tag{2.38}
$$

where $P_{i1}(y_1, y_2, \epsilon)$ $(i = 1, 2)$ is C^∞ and $P_{i1}(y_1, y_2, \epsilon) = O(|(y_1, y_2)|^3)$.

Using the transformation (2.33) (i.e., $u_1 = y_1$ and u_2 equals the right-hand side of the first equation in system (2.38)), we have

$$
\begin{aligned}
\frac{du_1}{dt} &= u_2,\\
\frac{du_2}{dt} &= g_{00}(\epsilon) + g_{10}(\epsilon)u_1 + g_{01}(\epsilon)u_2 + \frac{1}{2}g_{20}(\epsilon)u_1^2 + g_{11}(\epsilon)u_1u_2 + \frac{1}{2}g_{02}(\epsilon)u_2^2\\
&\quad + P_{22}(u_1, u_2, \epsilon),
\end{aligned}
\tag{2.39}
$$

where $P_{22}(y_1, y_2, \epsilon) = O(|(y_1, y_2)|^3)$, and

$$
\begin{aligned}
g_{00}(\epsilon) &= b_{00}(\epsilon)C(N^*, 0) + \cdots,\\
g_{10}(\epsilon) &= b_{10}(\epsilon)C(N^*, 0) + a_{11}(\epsilon)b_{00}(\epsilon) - b_{11}(\epsilon)a_{00}(\epsilon) + \cdots,\\
g_{01}(\epsilon) &= b_{01}(\epsilon) + a_{10}(\epsilon) - \frac{a_{11}(\epsilon)a_{00}(\epsilon)}{C(N^*, 0)} + \cdots,
\end{aligned}
$$

$$g_{20}(0) = b_{20}(0),$$
$$g_{11}(0) = a_{20}(0),$$
$$g_{02}(0) = 0.$$

Since $a_{kl}(\epsilon)$ and $b_{kl}(\epsilon)$ vanish at $\epsilon = 0$ for all $k + l \leqslant 1$, the terms shown above are sufficient for computing the first partial derivatives with respect to ϵ at $\epsilon = 0$.

Let

$$v_1 = u_1 - \delta(\epsilon), \qquad v_2 = u_2,$$

then the above system becomes

$$\begin{aligned}
\frac{dv_1}{dt} &= v_2,\\
\frac{dv_2}{dt} &= g_{00}(\epsilon) + g_{10}(\epsilon)\delta(\epsilon) + \big(g_{10}(\epsilon) + g_{20}(\epsilon)\delta(\epsilon) + O\big(\delta^2\big)\big)v_1\\
&\quad + \big(g_{01}(\epsilon) + g_{11}(\epsilon)\delta(\epsilon) + O\big(\delta^2\big)\big)v_2 + \frac{1}{2}\big(g_{20}(\epsilon) + O(\delta)\big)v_1^2\\
&\quad + \big(g_{11}(\epsilon) + O(\delta)\big)v_1 v_2 + P_{32}(v_1, v_2, \epsilon),
\end{aligned} \tag{2.40}$$

where $P_{32}(v_1, v_2, \epsilon) = O(|(v_1, v_2)|^3)$. Since

$$g_{20}(0) = b_{20}(0) = B\bar{C}''(N^*)P^* < 0,$$

there exists a smooth function

$$\delta(\epsilon) \approx -\frac{g_{10}(\epsilon)}{g_{20}(0)},$$

annihilating the term proportional to v_1 in the equation for v_2, which leads to the following system:

$$\begin{aligned}
\frac{dv_1}{dt} &= v_2,\\
\frac{dv_2}{dt} &= h_{00}(\epsilon) + h_{01}(\epsilon)v_2 + \frac{1}{2}h_{20}(\epsilon)v_1^2 + h_{11}(\epsilon)v_1 v_2 + P_{42}(v_1, v_2, \epsilon),
\end{aligned} \tag{2.41}$$

where $P_{42}(v_1, v_2, \epsilon) = O(|(v_1, v_2)|^3)$ is C^∞. Notice that

$$h_{00}(\epsilon) = g_{00}(\epsilon) + \cdots, \qquad h_{01}(\epsilon) = g_{01}(\epsilon) - \frac{g_{10}(\epsilon)}{g_{20}(0)}g_{11}(\epsilon) + \cdots,$$

and

$$h_{20}(0) = g_{20}(0) < 0, \qquad h_{11}(0) = g_{11}(0) < 0.$$

Introduce the scaled time,

$$s = \left| \frac{h_{11}(\epsilon)}{\frac{1}{2}h_{20}(\epsilon)} \right| t,$$

and scaled variables,

$$z_1 = \frac{h_{11}(\epsilon)}{(\frac{1}{2}h_{20}(\epsilon))^2} v_1, \qquad z_2 = \frac{h_{11}^2(\epsilon)}{(\frac{1}{2}h_{20}(\epsilon))^3} v_2.$$

Notice that the denominators are nonzero at $\epsilon = 0$. System (2.41) then takes the following form:

$$\begin{aligned} \frac{dz_1}{ds} &= z_2, \\ \frac{dz_2}{ds} &= \mu_1(\epsilon) + \mu_2(\epsilon) z_2 + z_1^2 + z_1 z_2 + P_{52}(z_1, z_2, \epsilon), \end{aligned} \tag{2.42}$$

where $P_{52}(z_1, z_2, \epsilon) = O(|(z_1, z_2)|^3)$ is C^∞, and

$$\begin{aligned} \mu_1(\epsilon) &= \frac{(\frac{1}{2}h_{20}(\epsilon))^4}{h_{11}^3(\epsilon)} h_{00}(\epsilon) = \frac{(\frac{1}{2}b_{20}(0))^4}{(a_{20}(0))^3}(B\epsilon_1 - \epsilon_2) G P^* + O\big(|\epsilon|^2\big), \\ \mu_2(\epsilon) &= \frac{(\frac{1}{2}h_{20}(\epsilon))^2}{h_{11}^2(\epsilon)} h_{01}(\epsilon) \\ &= \frac{(\frac{1}{2}b_{20}(0))^2}{(a_{20}(0))^2}\left[\left(B - \frac{GK^2 e\alpha}{2} - \frac{(-2\alpha + hG)^2 Ge}{\alpha}\right)\epsilon_1 - \epsilon_2\right] + O\big(|\epsilon|^2\big). \end{aligned} \tag{2.43}$$

After checking that

$$\left.\frac{D(\mu_1, \mu_2)}{D(\epsilon_1, \epsilon_2)}\right|_{(\epsilon_1 = 0,\, \epsilon_2 = 0)} > 0,$$

we know that system (2.35) (with parameters ϵ_1 and ϵ_2) is a generic family unfolding at the codimension 2 cusp singularity. This completes the proof. □

For system (2.42), the saddle-node bifurcation is given by (2.42)

$$\text{SN:} \quad \mu_1(\epsilon) = 0,$$

or in (ϵ_1, ϵ_2) is

$$\epsilon_2 = B\epsilon_1 + O\big(\epsilon_1^2\big). \tag{2.44}$$

We remark that (2.44) is consistent with the saddle-node bifurcation computed directly from the original system which, by using (2.34) and (2.35), is given by

$$\epsilon_2 = B\epsilon_1.$$

The Hopf bifurcation curve for system (2.42) is

$$\mu_2 = \sqrt{-\mu_1}, \quad \text{for } \mu_1 < 0,$$

which in (ϵ_1, ϵ_2) is

$$\epsilon_2 = B\epsilon_1 - \frac{2(2 + e\sigma_0 hK)^5 B}{(4 + e\sigma_0 hK)^2 h^2 (e\sigma_0)^3 K^3}\epsilon_1^2 + O\big(|\epsilon|^3\big).$$

This can also be shown to be consistent with the Hopf curve given in (2.22).

From dynamical systems theory we know that bifurcations of (2.35) near $(\mu_1, \mu_2) = (0, 0)$ are also present in the original system (1.1) near $(G, d) = (\hat{G}, \hat{d})$. From the properties of the Takens–Bogdanov bifurcation we know that, besides the saddle node and Hopf bifurcations, system (2.35) has a homoclinic bifurcation near $(\mu_1, \mu_2) = (0, 0)$. The existence of a homoclinic bifurcation is given in the following result.

Theorem 4. *For (G, d) sufficiently close to $(\hat{G}, \hat{d})$, the system* (1.1) *has a homoclinic bifurcation along the curve $d = d_{\text{hom}}(G)$, which is defined by*

$$d_{\text{hom}}(G) = \hat{d} + \frac{5}{7}\left(B\epsilon_1 - \frac{2(2 + e\sigma_0 hK)^5 B}{(4 + e\sigma_0 hK)^2 h^2 (e\sigma_0)^3 K^3}\epsilon_1^2\right) + O\big(\epsilon_1^3\big) \tag{2.45}$$

with $\epsilon_1 = G - \hat{G}$.

Proof. For system (2.42), using results in [11] for the Takens–Bogdanov bifurcation, we know that there is a homoclinic curve given by

$$\mu_2 = \frac{5}{7}\sqrt{-\mu_1}, \quad \text{for } \mu_1 < 0,\ |\mu_1| \ll 1.$$

The corresponding curve in (G, d) is the one given in (2.45), which is located below the Hopf curve. The proof is finished. □

Figure 5 illustrates the location of the homoclinic curve $d_{\text{hom}}(G)$ in the (G, d) plane. We remark that from the above result we only have the homoclinic curve $d_{\text{hom}}(G)$ near the cusp point O_p (e.g., the solid portion shown in Fig. 5). In the next subsection we discuss the possible extension of this curve.

2.4. Global dynamics and bifurcation diagram for system (1.1)

All bifurcations identified in the previous subsection are local results. We now use these results to obtain information about global dynamics and bifurcations.

First, as shown in Fig. 5, the bifurcation curves $\bar{d}(G)$, $d_k(G)$, and $d_{\text{hopf}}(G)$ divide the region Ω into following sub-regions: I (which is $I_1 \cup I_2$), II, III_1 (which is $III_{1a} \cup III_{1b}$), and III_2. From the result of Hopf bifurcation we know that for $(G, d) \in I_1$ and near the curve $d_{\text{hopf}}(G)$, a stable periodic solution exists. The following result shows that the existence of periodic solutions can be extended to the whole region I_1.

Theorem 5. *System* (1.1) *has at least one stable limit cycle for any* $(G, d) \in I_1$.

Proof. First, define the positive region $\mathcal{D} = \{(N, P) \mid 0 < N < K,\ 0 < P < \bar{P}\}$, where $\bar{P}$ is some positive number. It is easy to verify that the region $\mathcal{D}$ is invariant for system (1.1) for an appropriate $\bar{P}$. For any $(d, G) \in I_1$, system (1.1) has two boundary equilibria $E_0 = (0, 0)$ and $E_K = (K, 0)$, both of which are saddle, and an interior equilibrium E_1^* which is a repeller. By the Poincaré–Bendixson theorem, there exists at least one stable limit cycle. □

Numerical simulations suggest that the stable limit cycle is unique. It is beyond the scope of this paper to prove analytically the uniqueness of the limit cycle.

For the homoclinic curve $d_{\text{hom}}(G)$, the solid part is given in (2.45) which is defined for (G, d) close to $O_p = (\hat{G}, \hat{d})$. We know that for (G, d) below (or to the left of) the curve (the solid part) there is no periodic solution, and that for (G, d) above (or to the right of) the solid curve there is one stable periodic solution. Our intensive numerical simulations indicate that this curve can be extended as shown by the dashed curve in Fig. 5, which divides the region III_1 into $III_{1\text{a}}$ and $III_{1\text{b}}$, such that there is no periodic solution in $III_{1\text{a}}$ and there is one stable periodic solution in $III_{1\text{b}}$. From the above analysis we obtain Fig. 5, which describes a global bifurcation diagram and depicts the phase portraits in each of the regions.

2.5. Numerical simulations

The numerical simulations of the system (1.1) for the case of constant $\sigma(N)$ not only confirm our analytic results, but also help extend the local results to get a global bifurcation diagram. In the simulations presented in this section, all parameter values are fixed and only G and d are varied so that (G, d) is chosen from different subregions in the bifurcation diagram (5). The parameter values are: $r = 0.01$, $K = 1\,700\,000$, $h = 1/200$, $e\sigma_0 = 0.0003$, and $B = 0.00003$. For this set of parameter values, we have $\hat{G} \approx 56$.

In Fig. 6, we fix the value of $G = 60$, which is slightly greater than $\hat{G}$, and choose six different d values corresponding to six points on a vertical line (in the (G, d) plane) which starts in region III_2 and passes through regions $III_{1\text{b}}$ and $III_{1\text{a}}$. This line also intersects both the solid and dashed parts of the homoclinic curve $d_{\text{hom}}(G)$. In all cases (a)–(f), we observe that there are two interior equilibria with E_2^* (the one with a larger N component) being a saddle and that the boundary equilibrium $E_K = (K, 0)$ is locally asymptotically stable. Figure 6(a) is for $(G, d) \in III_2$ and it shows that E_1^* is a stable focus. Figure 6(b) shows that when d is decreased so that (G, d) is in region III_2 (and above the solid part of $d_{\text{hom}}(G)$), E_1^* becomes unstable and a stable periodic solution appears via Hopf bifurcation. When d decreases further and (G, d) reaches the solid part of $d_{\text{hom}}(G)$, the periodic solution disappears and there is a homoclinic orbit as shown in Fig. 6(c). Figure 6(d) is for (G, d) in region $III_{1\text{a}}$, in which both E_1^* and E_2^* are unstable and there is no limit cycle. The boundary equilibrium E_K is the only attractor. As d continues to decrease, (G, d) reaches $d_{\text{hom}}(G)$ again (the dashed part) and it shows in Fig. 6(e) that there is a homoclinic orbit. Figure 6(f) shows that a stable periodic solution appears again after (G, d) passes $d_{\text{hom}}(G)$ and enters the region $III_{1\text{b}}$.

In Fig. 7 we fix $G = 90$, which is close to $G = 1/2h = 100$. Two values of d are chosen so that (G, d) is slightly above the curve $d_{\text{hopf}}(G)$ for one d value and slightly below for the other d value (i.e., (G, d) is in the region I_2 and I_1, respectively). We observe that in both cases there is only one interior equilibrium E_1^* and that the boundary equilibrium E_K is unstable. Figure 7(a) is for $(G, d) \in I_2$ and it shows that E_1^* is stable. Figure 7(b) is for $(G, d) \in I_1$ and it shows that

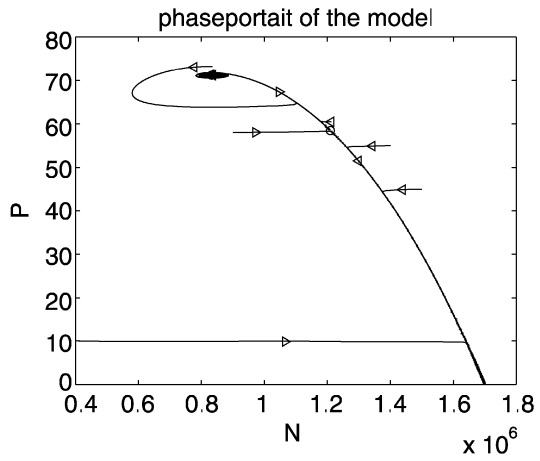

(a) $d = 0.00179$ and $(G, d) \in III_2$.

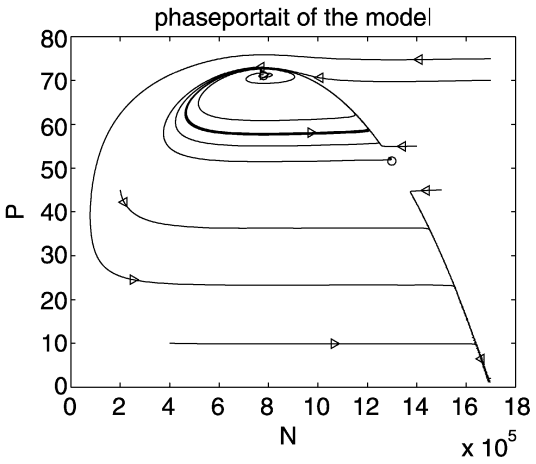

(b) $d = 0.0017815$ and $(G, d) \in III_{1\mathrm{b}}$.

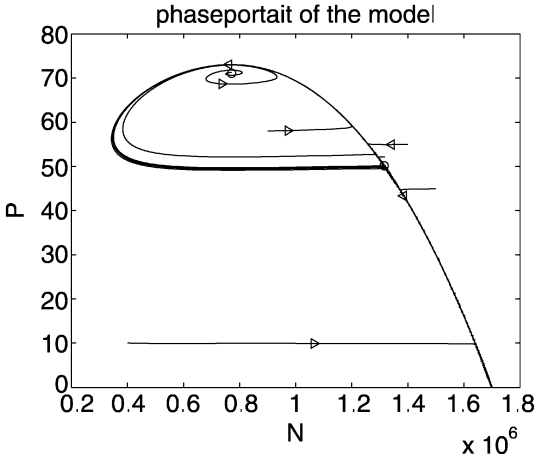

(c) $d = 0.001779$, (G, d) is on $d_{hom}(G)$.

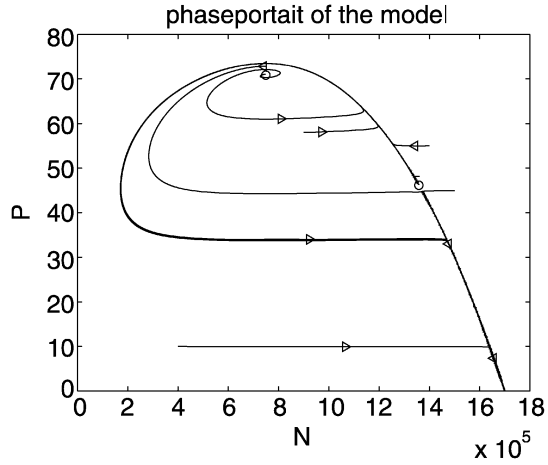

(d) $d = 0.001775$ and $(G, d) \in III_{1\mathrm{a}}$.

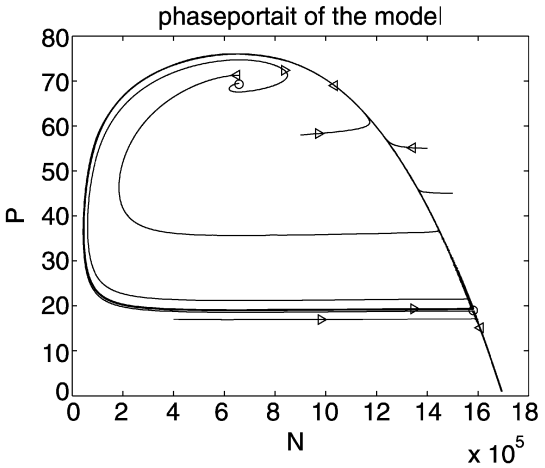

(e) $d = 0.0017465$, (G, d) is on $d_{hom}(G)$.

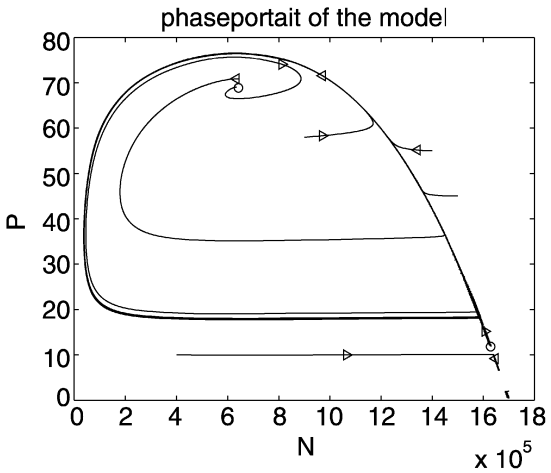

(f) $d = 0.00174$ and $(G, d) \in III_{1\mathrm{b}}$.

Fig. 6. Simulation results for system (1.1). $G = 60$ is fixed which is slightly greater than $\hat{G}$. The value of d decreases so that (G, d) moves along a vertical line passing through regions III_2, $III_{1\mathrm{b}}$, $III_{1\mathrm{a}}$, as well as the homoclinic curve $d_{\mathrm{hom}}(G)$. These phase portraits confirm our bifurcation analysis (see the text for more discussions).

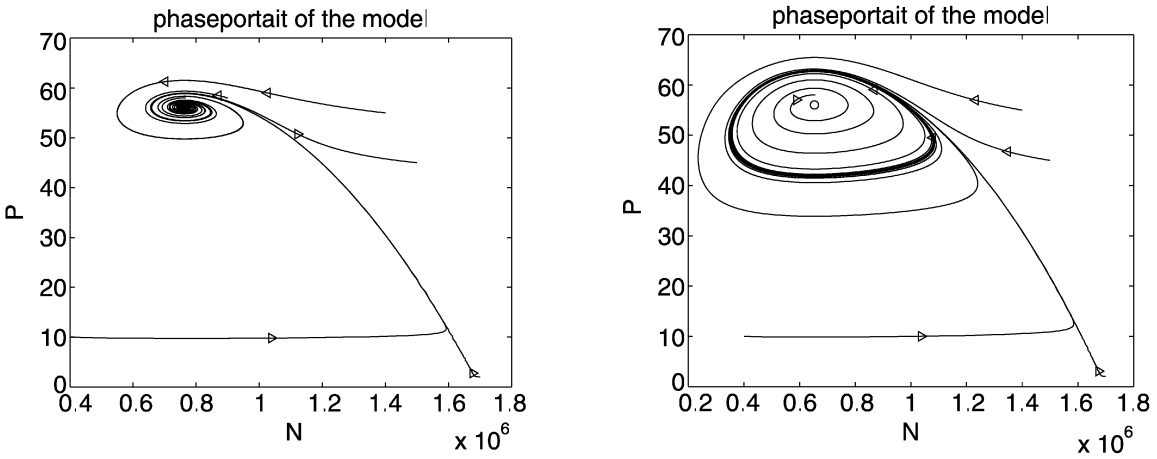

(a) $d = 0.0022531$ and $(G, d) \in I_2$. (b) $d = 0.0021531$ and $(G, d) \in I_1$.

Fig. 7. Simulation results for system (1.1) when $G = 90$, which is close to $G = 1/2h = 100$. Two values of d are chosen so that (a) (G, d) is slightly above the curve $d_{\text{hopf}}(G)$ in region I_2, and (b) (G, d) is slightly below the curve $d_{\text{hopf}}(G)$ in region I_1. Other parameters have the same values as in Fig. 6. It illustrates that, as d decreases and passes through d_{hopf}, the interior equilibrium E_1^* changes from being stable (see (a)) via a Hopf bifurcation and a stable periodic solution exists (see (b)).

E_1^* is unstable and a stable periodic solution appears via Hopf bifurcation. Other parameters have the same values as in Fig. 6.

3. Analysis of model (1.1) for the case of non-constant $\sigma(N)$

In this section, we consider the case in which the herbivore can control its rate of consumption of plant items. It is assumed that the herbivore can decide whether or not to consume an encountered food item, and especially to limit ingestion when the plant density N is high. For example, the herbivore can adjust $\sigma(N)$ so that $\sigma(N) \propto N_m/N$ when $N > N_m$, where $N_m = \frac{2G}{e\sigma_0(1-2hG)}$ is the plant density at which $C(N)$ has its maximum G. A more detailed discussion on this assumption is given in [4]. Following [4], we consider the following form for $\sigma(N)$:

$$\sigma(N) = \begin{cases} \sigma_0, & \text{for } N \leqslant N_m, \\ \sigma_0 \frac{N_m}{N}, & \text{for } N_m < N \leqslant K, \end{cases} \tag{3.1}$$

where σ_0 is a constant. Let $C_1(N)$ be the corresponding function for the non-constant $\sigma(N)$ given in (3.1), i.e.,

$$C_1(N) = \begin{cases} C(N, \sigma_0), & \text{for } N \leqslant N_m, \\ G, & \text{for } N > N_m, \end{cases} \tag{3.2}$$

where $C(N, \sigma_0)$ is given in (1.2) with $\sigma = \sigma_0$. Rewrite system (1.1) as

$$\begin{aligned} \frac{dN}{dt} &= rN\left(1 - \frac{N}{K}\right) - C_1(N)P, \\ \frac{dP}{dt} &= BC_1(N)P - dP. \end{aligned} \tag{3.3}$$

Clearly, $C_1(N)$ is continuously differentiable, and hence, the existence and uniqueness of solutions are guaranteed.

The dynamics of the system (3.3) are very different from that of (1.1). System (3.3) still has two boundary equilibria, $E_0 = (0,0)$ and $E_K = (K,0)$. It is easy to show that E_0 is always a saddle. The stability of E_K is determined by the sign of $BC_1(K) - d$, which determines a bifurcation curve $\tilde{d}_K(G)$:

$$\tilde{d}_K(G) = \begin{cases} B(G - C_1(K)), & \text{for } G > G_c \text{ (in this case } K < N_m), \\ BG, & \text{for } G < G_c \text{ (in this case } K > N_m), \end{cases} \tag{3.4}$$

where G_c is given in (2.10). For $G > G_c$, E_K is l.a.s. if $d > \tilde{d}_K$, and unstable if $d < \tilde{d}_K$. For $G < G_c$, E_K is always unstable.

Since the function $C_1(N)$ is monotone, there is at most one feasible interior equilibrium, which we denote by $E^* = (N^*, P^*)$, with $0 < N^* < K$ and $P^* > 0$. Let $g_1(N) = rN(1 - N/K)/C_1(N)$, then the first equation in (3.3) can be written as

$$\frac{dN}{dt} = C_1(N)\big(g_1(N) - P\big).$$

The graph of $g_1(N)$ has properties similar to that of $g(N)$ (see Fig. 2). Clearly, N^* and P^* at the interior equilibrium E^* are solutions of the equations

$$BC_1(N) = d \quad \text{and} \quad P = g_1(N), \tag{3.5}$$

with $0 < N^* < K$. Also, since $C_1(N) \equiv G$ for all $N \geqslant N_m$, we also have that $N^* < N_m$.

Noticing that $C_1(N) = C(N)$ for all $N \leqslant N_m$, we know that N^* (which must be smaller than N_m) is given by the same expression as N_1^* in the case of constant $\sigma(N)$. Thus, similarly to the case of constant $\sigma(N)$, we can show that the existence condition of E^* is related to the stability of E_K, which is determined by the bifurcation curve $\tilde{d}_K(G)$. That is, N^* exists if $d < \tilde{d}_K(G)$ and it does not exist if $d \geqslant \tilde{d}_K(G)$.

From $N^* < N_m$ and $C_1(N) = C(N)$, $g_1(N) = g(N)$ for all $N \leqslant N_m$, we know that the Jacobian at E^* is the same as the Jacobian at E_1^*. It follows that the stability of E^* is determined by the sign of $g'(N^*)$. That is, E^* is stable if $g'(N^*) < 0$ and unstable if $g'(N^*) > 0$. Hence, the stability of E^* is the same as the stability of E_1^* for (1.1), and hence, a supercritical Hopf bifurcation occurs along the curve $d_{\text{hopf}}(G)$ given in (2.22).

The curves $\bar{d}(G)$, $\tilde{d}_K(G)$, and $d_{\text{hopf}}(G)$ divide Ω into four sub-regions: I_1, I_2, II, and III as shown in Fig. 8, which is very different from Fig. 5 for the case when $\sigma(N)$ is constant. In particular, region III in Fig. 8 is much simpler than the region III $(= III_{1a} \cup III_{1b} \cup III_b)$ in Fig. 5. The reason for this is that homoclinic bifurcation is not possible because of the absence of a saddle-node bifurcation for (3.3). Moreover, since the curves $\tilde{d}_K(G)$ and $\bar{d}(G)$ are the same for $G < G_c$, regions III_{1b} and III_b are not present. Region III is determined by the vertical line $G = \hat{G}$.

Stability results in regions I_2 and II follow from the local stability analysis for E_K and E^* as mentioned above. For the region I_1, using the similar argument as for the case of constant $\sigma(N)$ we know that the existence of a stable limit cycle near the Hopf curve $d_{\text{hopf}}(G)$ can be extended

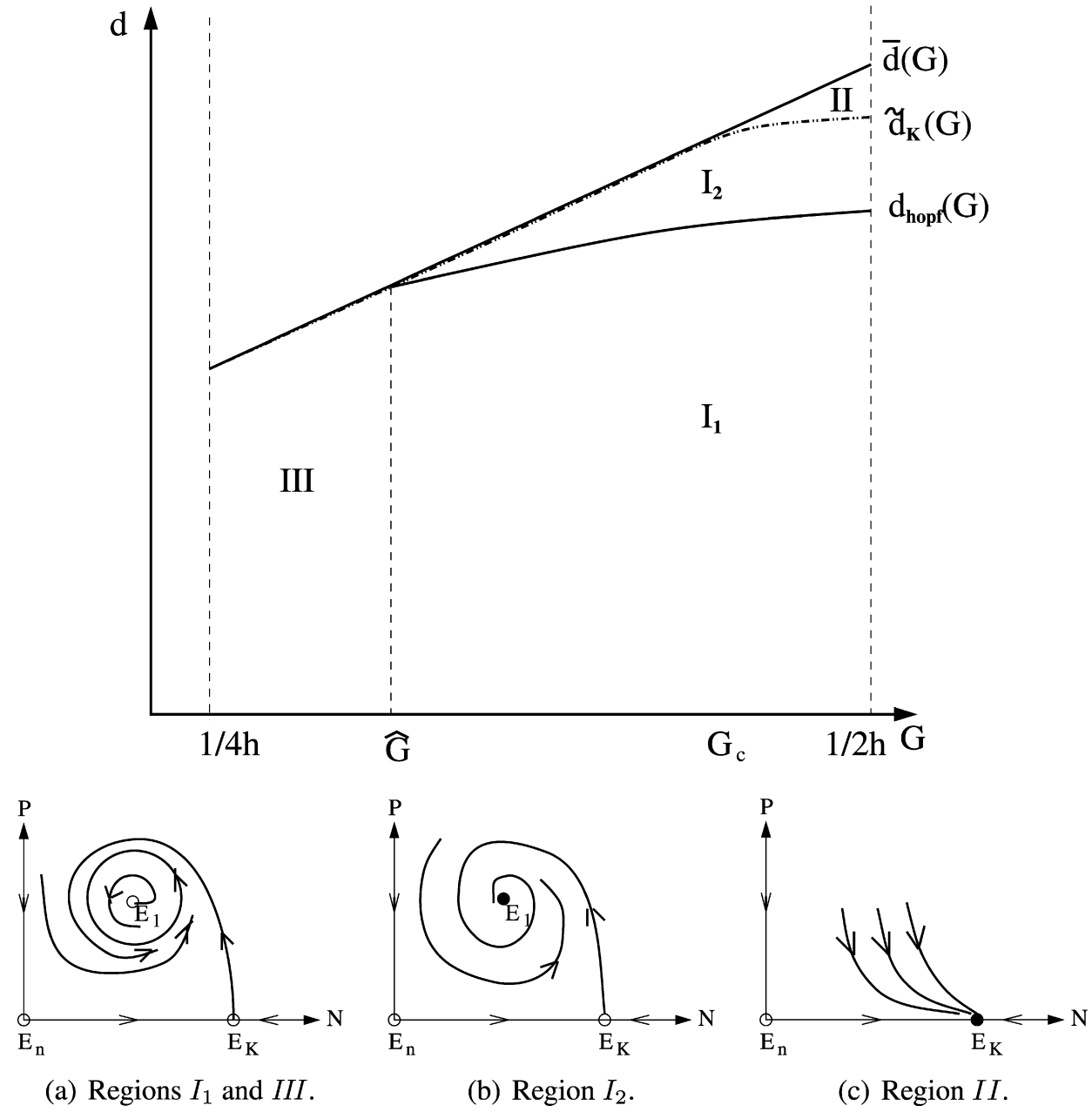

(a) Regions I_1 and III. (b) Region I_2. (c) Region II.

Fig. 8. The top panel is a bifurcation diagram for the case where $\sigma(N)$ is not constant and has the form given in (3.1). The bottom panel are phase portraits for (G, d) in various regions.

to the whole region. However, the behaviors of system (3.3) in region *III* is very different from that of (1.1). In fact, the following result holds.

Theorem 6. *System* (3.3) *has a stable periodic solution for all* $(G, d) \in III$ *in Fig.* 8.

Proof. Notice that the region $D = \{(N, P) \mid 0 \leqslant N < A,\ 0 \leqslant P < A\}$, where $A > K$ is a large positive number, is positively invariant. For $(G, d) \in III$ the system (3.3) has two boundary equilibria, $E_0 = (0, 0)$ and $E_K = (K, 0)$, both of which are saddle points, and an interior equilibrium, E^*, which is a repeller. Notice also that the N-axis is an invariant manifold of E_0 and E_K. Therefore, there is no graphic in the region D. From the Poincaré–Bendixson theorem, there must exist a stable periodic orbit in D for all $(G, d) \in III$. □

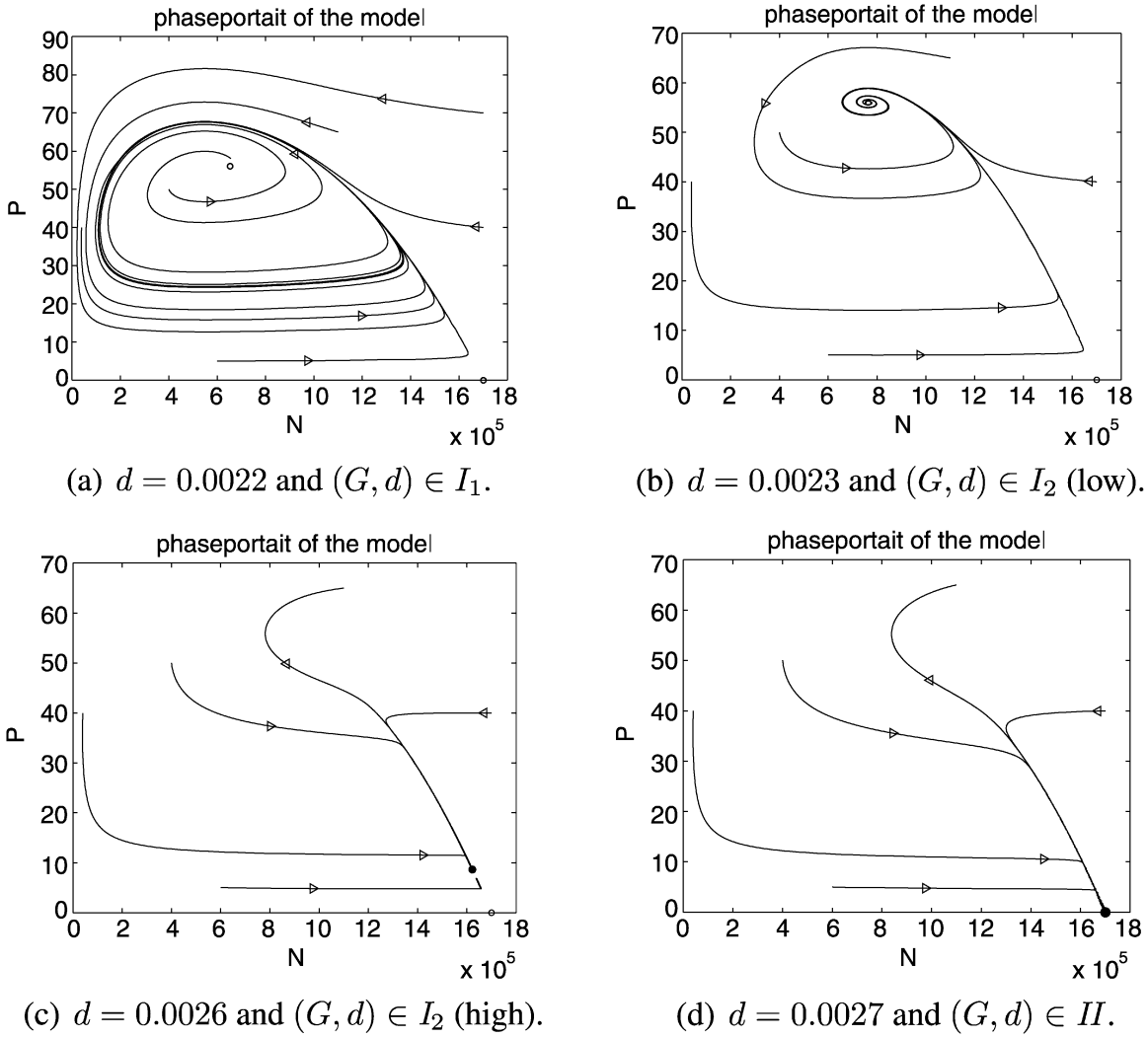

(a) $d = 0.0022$ and $(G, d) \in I_1$. (b) $d = 0.0023$ and $(G, d) \in I_2$ (low).

(c) $d = 0.0026$ and $(G, d) \in I_2$ (high). (d) $d = 0.0027$ and $(G, d) \in II$.

Fig. 9. Simulation results for system (3.3). All parameter values except G and d are the same as in Fig. 6. G is chosen to be 90 which is near $G = 1/2h = 100$. d varies so that (G, d) is in various regions. (a) shows that in region I_1, E_1^* (marked by a circle) and E_K are unstable, and there is a periodic solution. (b) and (c) show that in region I_2, E_1^* is a stable focus for larger d and a stable node for smaller d, and the periodic solution disappears due to the Hopf bifurcation. (d) shows that in region II there is no interior equilibrium and E_K is a global attractor.

As is in the case of constant $\sigma(N)$ we know that for all $(G, d) \in I_1$ there is a stable periodic solution. Also, in region II there is no interior equilibrium and the boundary equilibrium E_K is stable. Figure 8 describes the global bifurcation diagram and phase portraits of system (3.3).

Numerical simulations have also been carried out for system (3.3), some of which are illustrated in Figs. 9 and 10. These figures are produced by varying the values of G and d with all other parameters having the same values as in Figs. 6 and 7.

In Fig. 9, we fix the value of G at $G = 90$ (which is near $1/2h = 100$) and vary d such that (G, d) belongs to either region I_1, or I_2, or II. We observe that a stable periodic solution exists in region I_1 while E_1^* and E_K are both unstable (see (a)). In (b) it shows that when d is increased and (G, d) just passes $d_{\text{hopf}}(G)$ and enters region I_2, the periodic solution disappears and E_1^* becomes a stable focus. As d continues to increase and (G, d) approaches the curve $d_K(G)$, E_1^* becomes a stable node (see (c)). Finally, when (G, d) enters the region II, the interior equilibrium E_1^* disappears and E_K is a global attractor.

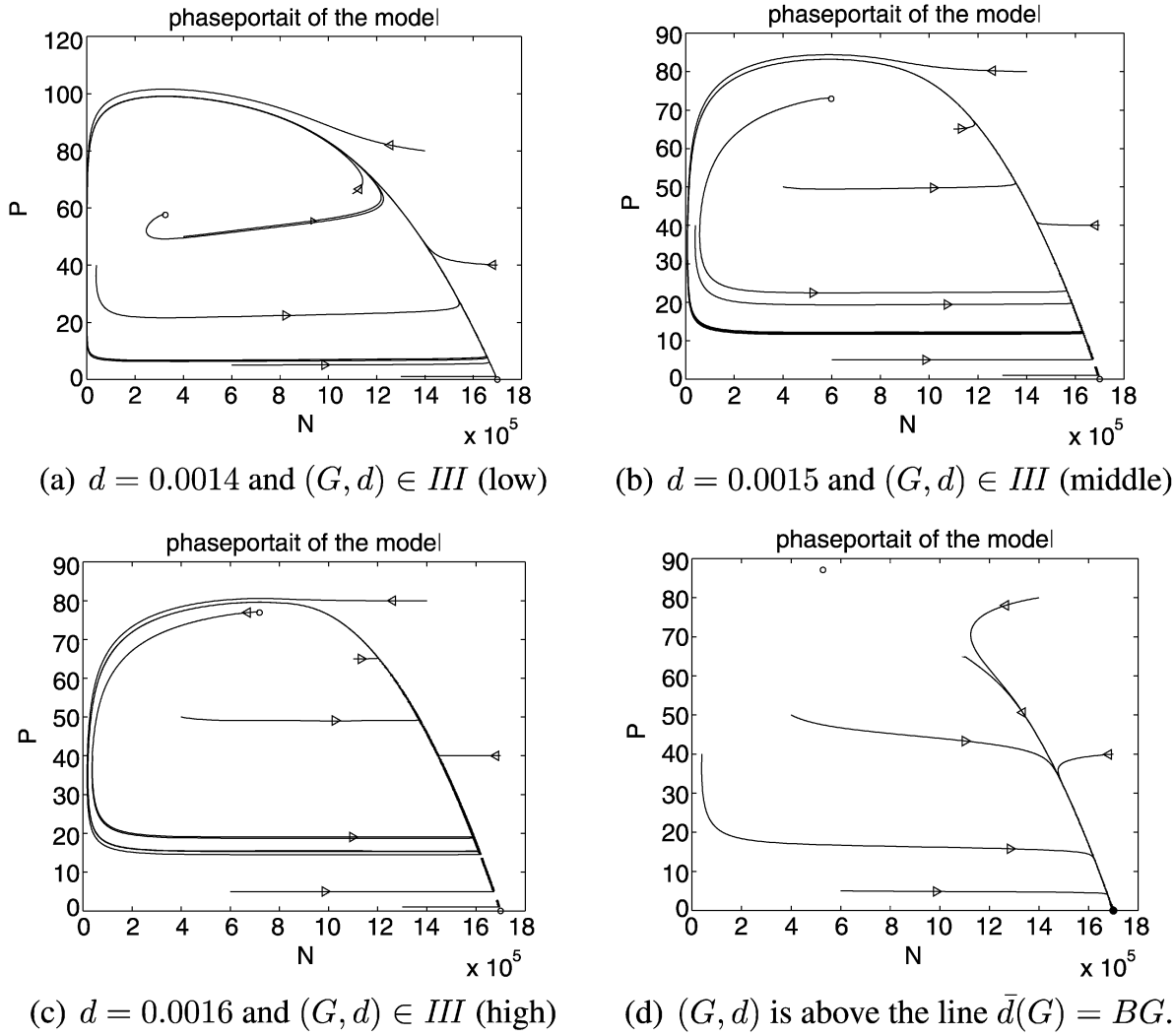

Fig. 10. G is chosen to be 54, which is to the left of $\hat{G} \approx 56$. d varies so that (G, d) is in various part of region *III*. (a)–(c) show that for all $d \in (0, \bar{d})$, as long as $(G, d) \in III$, E_1^* (marked by a circle) and E_K are unstable and the system (3.3) has a stable periodic solution. (d) shows that for $d > \bar{d}$ there is no periodic solution and E_K is a global attractor.

Figure 10 illustrates the dynamics when $G = 54$ which is to the left of $\hat{G}$. (a)–(c) show that for $(G, d) \in III$ there is always a stable limit cycle. (d) shows that when (G, d) is above the line $\bar{d}(G) = BG$, there is neither limit cycle nor interior equilibrium, while E_K is a global attractor.

These simulation results are clearly consistent with the results obtained from the bifurcation analysis.

4. Conclusion

In this paper, we study the dynamics of the system (1.1), which models plant–herbivore interactions with a functional response mediated by plant toxicity. This toxin-determined functional response model (1.1) (referred to as TDFRM) is a modification of the traditional consumer-resource model with Holling Type II functional response, and the modification is biologically well-justified (see [4,8]).

We show that the TDFRM is capable of producing much more complex dynamics than the Holling Type II functional response model. For instance, the TDFRM may have multiple attractors for parameter values in certain regions (e.g., a stable interior equilibrium and a stable limit

cycle in region III_{1b}, or two stable equilibria in region III_2), and both Hopf and homoclinic bifurcations are possible. The complex dynamics have important biological implications for the plant–herbivore interaction under the influence of plant toxicity (see [4] for a more detailed discussion).

To explore the impact of plant toxicity and toxin-determined herbivore browsing on the plant–herbivore dynamics, we conducted bifurcation analysis using G (which provides a measure of toxicity) and d (which affects the fitness of herbivores) as bifurcation parameters. We derived bifurcation curves which divide the parameter region Ω into several subregions. Existence and stability of equilibria and limit cycles in these subregions are presented. The existence of a homoclinic bifurcation is determined by identifying a cusp point of codimension 2 and applying the results for the Takens–Bogdanov bifurcation.

For the analysis of the TDFRM, we considered two cases in terms of the consumption choice coefficient $\sigma(N)$. In the first case, $\sigma(N) = \sigma_0$ is a constant for which the functional response function $C(N)$ is unimodal. In the second case, $\sigma(N)$ is a non-constant function given in (3.1) for which $C(N)$ is monotone. Both cases are biologically relevant, and which one is more appropriate will depend on whether the herbivore can have some control of its rate of consumption of plant items when that is likely to lead to lethal toxicant intake. Our results show that the dynamics of the TDFRM in the two cases are very different. In both cases, the model behaviors suggest that an effect of the toxicant is to increase the likelihood of the well-known 'paradox of enrichment' type limit cycle oscillations ([12]; see also [4] for a more detailed discussion).

The system considered in this article is a two-dimensional TDFRM. We have also studied a three-dimensional TDFRM which includes two plant species and one herbivore population (see [8]). The analytical results obtained in [8] are very limited. A more detailed bifurcation analysis of the 3-D system (similar to what has been done for the 2-D model in this paper) will be both mathematical challenging and biologically interesting.

Acknowledgment

We thank the reviewer for very helpful comments and suggestions which greatly improved the presentation of the paper.

References

[1] P.A. Abrams, Decreasing functional responses as a result of adaptive consumer behavior, Evol. Eco. Res. 3 (1989) 95–114.
[2] J.P. Bryant, F.S. Chapin III, D.R. Klein, Carbon/nutrient balance of boreal plants in relation to herbivory, Oikos 40 (1983) 357–368.
[3] J.P. Bryant, R.K. Swihart, P.B. Reichardt, L. Newton, Biogeography of woody plant chemical defense against snowshoe hare browsing: Comparison of Alaska and eastern North America, Oikos 70 (1994) 385–394.
[4] Z. Feng, R. Liu, D. DeAngelis, Plant–herbivore interactions mediated by plant toxicity, Theoret. Pop. Biol. (2007), accepted for publication.
[5] C.S. Holling, The components of predation as revealed by a study of small mammal predation on the European pine sawfly, Can. Ent. 91 (1959) 293–320.
[6] C.S. Holling, Some characteristics of simple types of predation and parasitism, Can. Ent. 91 (1959) 385–398.
[7] Y. Kuznetsov, Elements of Applied Bifurcation Theory, Springer-Verlag, 1998.
[8] Y. Li, Z. Feng, R. Swihart, J. Bryant, H. Huntley, Modeling plant toxicity on plant–herbivore dynamics, J. Dynam. Differential Equations 18 (4) (2006) 1021–1024.
[9] P. Lundberg, Functional response of a small mammalian herbivore: The disc equation revisited, J. Anim. Ecol. 57 (1988) 999–1006.

[10] P. Lundberg, M. Astrom, Functional response of optimally foraging herbivores, J. Theoret. Biol. 144 (1990) 367–377.
[11] L. Perko, Differential Equations and Dynamical Systems, Springer-Verlag, 1998.
[12] M.L. Rosenzweig, Paradox of enrichment: Destabilization of exploitation ecosystems in ecological time, Science 171 (1971) 385–387.
[13] D.E. Spalinger, T.A. Hanley, C.T. Robbins, Analysis of the functional response in the Sitka black-tailed deer, Ecology 69 (1988) 1166–1175.
[14] G. Wolkowicz, Bifurcation analysis of a predator–prey system involving group defence, SIAM J. Appl. Math. 48 (1988) 592–606.
[15] H. Zhu, S.A. Campbell, G. Wolkowicz, Bifurcation analysis of a predator–prey system with nonmonotonic function response, SIAM J. Appl. Math. 63 (2002) 636–682.